# Optical and Structural Properties of Cu Doped ZnS Nanocrystals: Effect of Temperature and Concentration of Capping Agent

J. Hasanzadeh*

Department of Physics, Takestan Branch, Islamic Azad University, Takestan, Iran

*(Received May 22, 2015)*

We have provided the Cu doped zinc sulfide (ZnS:Cu) nanoparticles using a wet chemical synthesis. In principle, the nanoparticles are provided by mixing the reactants in a double distilled water solvent. We have used the mercaptopropionic acid as the capping agent. We have obtained the physical properties of the nanoparticles using the methods: UV absorption, photoluminescence spectroscopy, and X-ray diffraction analysis. The average size of nanoparticles is obtained in the range 3–6 nm. In addition, the X-ray diffraction pattern of ZnS:Cu nanoparticles reveals a zinc-blende crystal structure at room temperature.

DOI: 10.12693/APhysPolA.129.1147

PACS/topics: 61.46.–w, 61.46.Hk, 78.67.Bf, 78.67.Hc

## 1. Introduction

Zinc sulfide is an important II–VI semiconductor with a wide band gap (3.7 eV [1]) which is suitable for applications in solar cells, solar selective decorative coatings, UV light emitting diode, photocatalysis, the phosphors in flat panel displays [2], electroluminescence [3], LED [4] and non-linear optical devices [5].

Variety of luminescence techniques such as thermoluminescence, electroluminescence, cathodoluminescence, X-ray irradiation, and ion beam luminescence can be used for excitation of luminescence [6].

In addition to these, doped semiconductor nanoparticles have tremendous potential to use in light emitting applications. These properties of nanocrystals make them a very interesting category of material for optoelectronic applications. These nanoparticles may find applications in nonlinear optical devices, photocatalysis etc. II–VI compound semiconductors have immense technological importance in different applied branches of the science and technology [7]. ZnS and ZnS:Cu are commercially used as catalysis [8–11], phosphorus and also in thin film electroluminescence devices [12, 13].

In recent years, accordingly, Mn-doped, Cu-doped and Mn and Cu-codoped ZnS powders have received much attention in research because many functions can be added by transporting and controlling numerous types of spin state [14–17].

ZnS particles have two kinds of structures: zinc blende structure (cubic crystal) and wurtzite structure (hexahedron). ZnS applied in luminescent materials generally has a zinc blende structure [18].

A variety of methods have been reported for synthesizing ZnS nanocrystals, such as the solvothermal method [19–21], single source molecular precursor [22, 23], the direct elemental reaction [24], the $\gamma$-irradiation [25], and rf-magnetron sputtering [26] and so on [27–31].

In a very recent work, we have studied the effect of thioglycerol (TG) concentration (as capping agent) on luminescence of Cu doped CdS nanoparticles previously [32]. In this paper, the aim of our research is to improve the synthesis method of Cu doped ZnS nanoparticles and study the effect of capping agent and the temperature on the physical properties of nanoparticles.

## 2. Experiment

### 2.1. Chemicals

Zinc chloride (anhydrous, Merck), copper chloride·$2H_2O$ and sodium sulfide·$xH_2O$ (Merck), mercaptopropionic acid (Fluka).

### 2.2. Synthesis

In a dry nitrogen atmosphere, 50 ml of $CuCl_2$ is added to 50 ml of an aqueous solution of $ZnCl_2$, whilst being stirred. Mercaptopropionic acid (MPA) is added dropwise into the mixture and an aqueous solution is also added as a surfactant in order to prevent nanoparticles agglomeration in the solution. Then 50 ml of $Na_2S$ solution is injected drop by drop into the above solution whilst being stirred. The final mixture is stirred for 60 min. The ZnS:Cu nanoparticles were then separated by centrifugation (3500 rpm for 10 min) and washed with acetone to get rid of any unreacted solvent. For drying, the particles are kept in a Petri dish for about 12 h. To investigate effects of the temperature, round-bottom flask (setup) is placed in the hot oil whose temperature is adjustable.

### 2.3. Characterization

Absorption spectra were measured using a Scan Cary 100 UV-vis spectrometer. X-ray diffraction (XRD) measurements were performed on a Philips PW 1840 diffractometer with Cu $K_\alpha$ radiation (40 kV, 40 mA), scan rate

*e-mail: j.hasanzadeh@tiau.ac.ir, j.hasanzadeh@yahoo.com

0.02 $2\theta$/s within a range of $2\theta$ of 20°–70°. XRD patterns were recorded using an automatic divergence slit system. The photoluminescence (PL) measurement was carried out at room temperature using Shimadzu RF-5000.

## 3. Results and discussion

### 3.1. Effect of capping agent

#### 3.1.1. Absorption spectra

Capping agents are used to stop the growth of nanoparticles and stabilize them from aggregation. The absorption spectra for freshly-prepared MPA-capped (different concentration) ZnS:Cu(1%) nanocrystals are shown in Fig. 1. This clearly shows that the absorption edge (excitonic peak) shifts towards shorter wavelengths as the capping agent concentration is decreased. The blue shift of absorption edges could be explained by the quantum confinement of ZnS:Cu nanocrystallites.

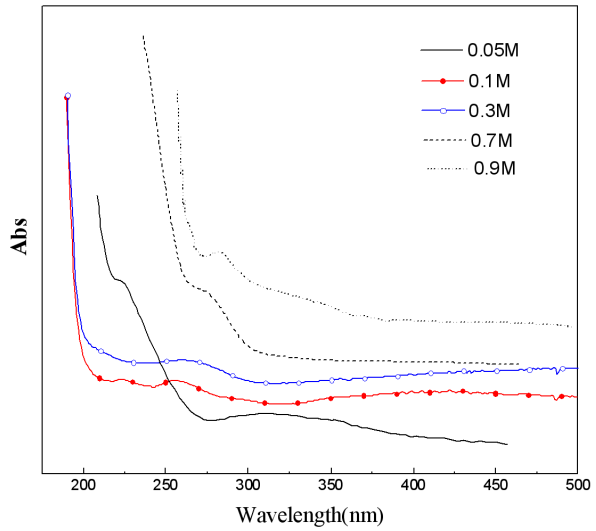


Fig. 1. Absorption spectra for ZnS:Cu (1%) nanoparticles prepared at different concentrations of MPA.

From the strong absorption edge, particle size has been assessed by using the Brus equation [33, 34]:

$$E_{\mathrm{gn}} = E_{\mathrm{gb}} + \frac{h^2}{8\mu R^2} - \frac{1.8e^2}{R}, \tag{1}$$

$$\frac{1}{\mu} = \frac{1}{m_{\mathrm{e}}^*} + \frac{1}{m_{\mathrm{h}}^*}. \tag{2}$$

Here, $R$ is quantum dot radius ($2R$ is the diameter and hence the particle size), $E_{\mathrm{gb}}$ is the bulk band gap, $E_{\mathrm{gn}}$ is quantum dot band gap (calculated from the strong absorption edge), $h$ is the Planck constant, $m_{\mathrm{e}}^*$ and $m_{\mathrm{h}}^*$ are effective mass of electron and hole, respectively. From (1) and (2) the particle size of samples can be determined (Table I) using the values of $\varepsilon = 8.76$, $m_{\mathrm{e}}^* = 0.34m_0$ and $m_{\mathrm{h}}^* = 0.23m_0$ [35].

#### 3.1.2. Luminescence

Effect of MPA concentration on photoluminescence spectra of ZnS:Cu(3%) nanoparticles was investigated (Fig. 2). As shown, the first peak in PL spectra (450 nm) arises from the recombination between the shallow donor (sulfur–vacancy) to the valence band. The second peak (461 nm) is attributed to transition from CB to the $t_2$ state of $Cu^{2+}$. The third peak (486 nm) is due to recombination between CB to trap states emission of ZnS ($V_{zn}$). The fifth peak (531 nm) arises from a shallow donor (sulfur-vacancy) to the $t_2$ state [36].

TABLE I

The particle optical size [nm] of ZnS:Cu (1%) nanoparticles prepared at different concentration of MPA.

| MPA | 0.05 M | 0.1 M | 0.3 M | 0.7 M | 0.9 M |
|---|---|---|---|---|---|
| size | 3.2 | 3.96 | 4.52 | 4.88 | 5.32 |

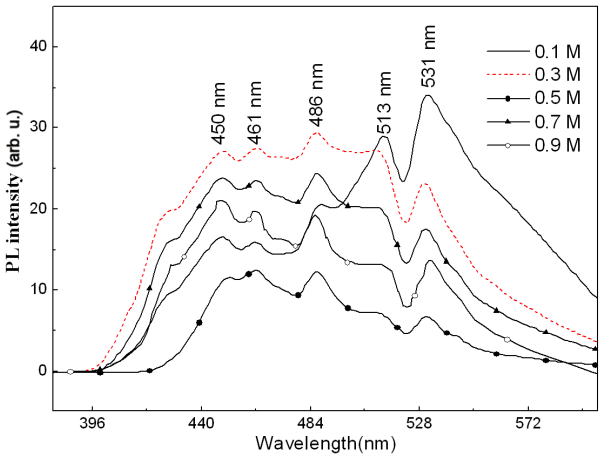


Fig. 2. PL spectra of ZnS:Cu(3%) nanoparicles in different concentration of capping agent prepared at room temperature.

### 3.2. Effect of temperature

#### 3.2.1. Absorption spectra

Figure 3 shows the absorption spectra of ZnS:Cu(3%) nanoparticles prepared at different temperature. We used 0.05 M $ZnCl_2$, $Na_2S$ and MPA and only changed the temperature of synthesis. As shown in Fig. 3, excitonic peak is broadened when temperature increases. Monodisperse nanoparticles are reachable at room temperature. The particle size of samples is determined as $\approx 3$ nm.

#### 3.2.2. X-ray diffraction

Figure 4 depicted XRD patterns of ZnS:Cu(3%) nanoparticles prepared at different temperature. As shown, for samples which were prepared at room temperature and 40 °C there are three diffraction peaks corresponding to the (111), (220), (311) planes, indicating a zinc-blende (ZB) crystal structure (JCPDS 05-0566, $a = 0.5406$ nm) which is the stable phase for room temperature bulk ZnS. Broadening of the XRD peaks indicates formation of ZnS nanocrystals.

The wurtzite structure (WZ) appeared in the samples that were synthesised at 60 and 80 °C. The wurtzite (100) peak is clearly visible next to the zinc blende (111) peak

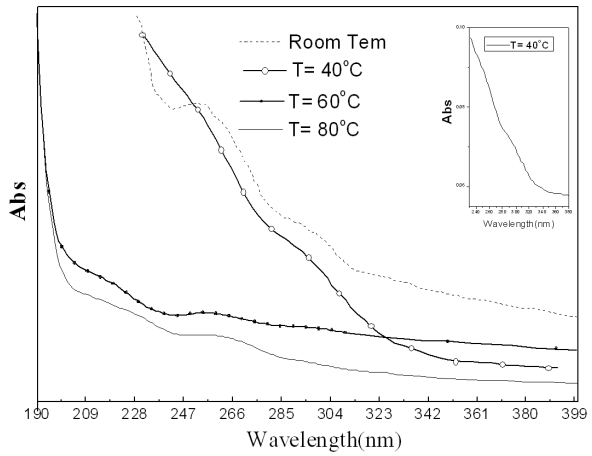


Fig. 3. UV-vis spectra of ZnS:Cu(3%) nanoparticles prepared at different temperature but in the same concentration of precursor.

in Fig. 4. Also we see at 40 °C that the wurtzite (101) peak currently appears which shows that zinc blende-to-wurtzite transition occurs at temperatures as low as 40 °C. These results are similar to Dinsmore et al. who reported coexistence of the two phases (zinc blende and wurtzite) after annealing at 400 and 525 °C, of course. They initially made ZnS:Mn powder and then annealed samples [37].

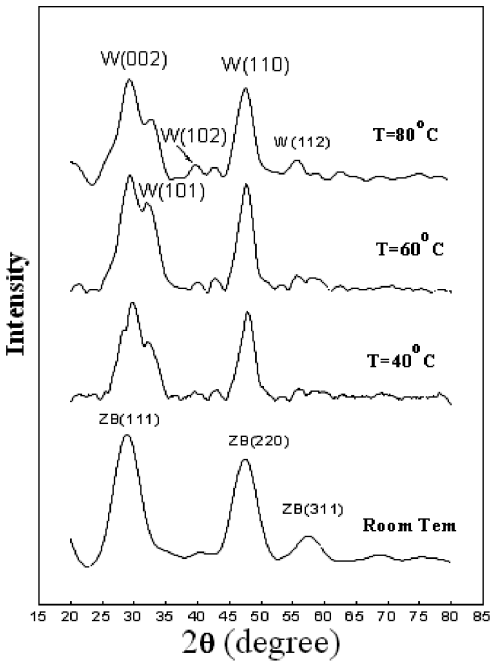


Fig. 4. XRD pattern of ZnS:Cu(3%) nanoparticles prepared at different temperature. After 60 and 80 °C, a coexistence of the two phases (zinc-blende and wurtzite) is observed.

The size of ZnS: Cu nanocrystals was approximately estimated by the Hall method [38]:

$$\frac{\beta\cos\theta}{\lambda} = \frac{1}{D} + \frac{2\varepsilon\sin\theta}{\lambda}, \tag{3}$$

where $\beta$ is the measured full width at half maximum (FWHM) in radians, $\theta$ is the Bragg angle of the diffraction peak, $\lambda$ is the X-ray wavelength, $D$ is the grain size, $\varepsilon$ is the effective residual strain.

Figure 5 represents a typical plot of $\frac{\beta\cos\theta}{\lambda}$ vs. $\frac{\sin\theta}{\lambda}$ for ZnS:Cu nanoparticles. $\varepsilon$ and $D$ can be estimated from the slope of the straight line and the intercept on $\frac{\beta\cos\theta}{\lambda}$ axis, respectively.

The estimated values for grain size and effective residual strain are given in Table II. The calculated values of the average grain sizes are slightly different from the optical sizes obtained from absorption spectra studies. This can be ascribed to the fact that the sub-$\mu$m particles are the aggregation of ZnS nanoparticles.

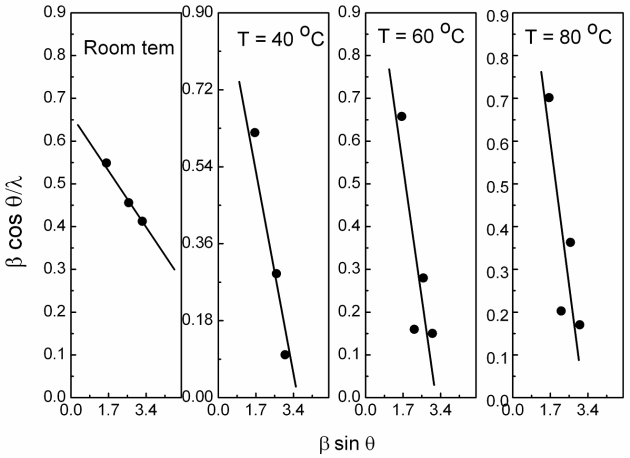


Fig. 5. Plot of $\beta\cos\theta/\lambda$ vs. $\sin\theta/\lambda$ for ZnS:Cu(3%) nanoparticles at different temperature.

TABLE II

Estimation of grain size [nm] and strain of ZnS:Cu(3%) nanoparticles at different temperature.

| Temperature | Grain size | Strain |
|---|---|---|
| R.T. | 1.5 | $4.2 \times 10^{-2}$ |
| $T = 40\,^{\circ}$C | 0.81 | $18.2 \times 10^{-2}$ |
| $T = 60\,^{\circ}$C | 0.93 | $16.05 \times 10^{-2}$ |
| $T = 80\,^{\circ}$C | 0.88 | $16.25 \times 10^{-2}$ |

*3.2.3. Luminescence*

In Fig. 6 PL spectra of ZnS:Cu(3%) nanoparticles prepared at different temperatures are shown. We can see that the PL intensity increased with increase of temperature. High intensity is related to $T = 40\,^{\circ}$C, although the PL intensity at $T = 80\,^{\circ}$C is almost like at $T = 40\,^{\circ}$C. Also, a new peak at 513 nm appears when the temperature increases. As shown in Figs. 2 and 6, there is another peak (the fourth peak) at 513 nm in MPA = 0.1 M (Fig. 2) and $T = 40$ and 80 °C (Fig. 5). This peak disappeared when concentration of MPA increased. This peak may be due to the variety of Cu complex which is sensitive to temperature and concentration of MPA.

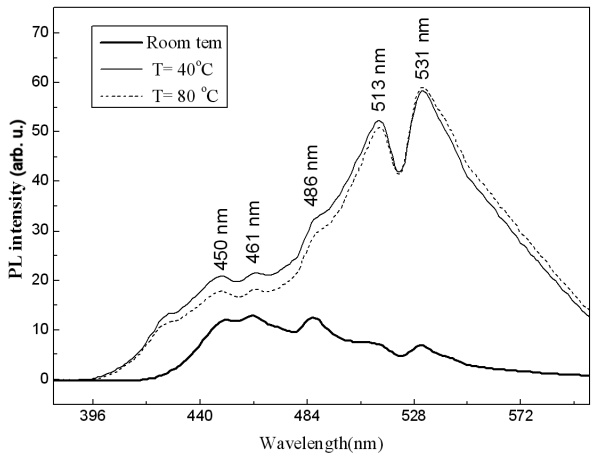


Fig. 6. PL spectra of ZnS:Cu(3%) nanoparticles prepared at different temperature.

## 4. Conclusions

We prepared the well dispersed ZnS:Cu nanoparticles using a wet chemical technique in doubled distilled water solution using MPA as capping reagent. We investigated the influence of capping agent concentration and the temperature on the absorption and emission spectra of the samples. The XRD results show that typical ZnS:Cu nanoparticles have the zinc-blende structure at room temperature. From absorption spectra, average size of samples was obtained in the range of 3–6 nm. Four band emissions were observed in the PL spectra due to recombination between the shallow donor (sulfur–vacancy) to the valence band, conduction band to the $t_2$ state of $Cu^{2+}$, conduction band to trap states emission of ZnS ($V_{zn}$) and shallow donor (sulfur–vacancy) to the $t_2$ state. We also observed another peak at 513 nm which disappeared when concentration of MPA increased.

## References

[1] *Phosphor Handbook*, Eds. W.M. Yen, S. Shionoya, CRC Press, Boca Raton, FL 1999.

[2] A. Kassim, S. Nagalingam, H.S. Min, N. Karrim, *Arab. J. Chem.* **3**, 243 (2010).

[3] E. Schlam, *Proc. IEEE* 61, 894 (1973).

[4] L. Sun, C. Liu, C. Liao, C. Yan, *J. Mater. Chem.* 9, 1655 (1999).

[5] J. Xu, W. Ji, *J. Mater. Sci. Lett.* 18, 115 (1999).

[6] P. Townsend, P. Chandler, L. Zhang, *Optical Effects of Ion Implantation*, Cambridge University Press, Cambridge 2006.

[7] J.P. Borah, K.C. Sarma, *Acta Phys. Pol. A* **114**, 713 (2008).

[8] A. Fukuoka, J.I. Kimura, T. Oshio, Y. Sakamoto, M. Ichikawa, *J. Am. Chem. Soc.* **129**, 10120 (2007).

[9] I.I. Slowing, B.G. Trewyn, S. Giri, V.S.Y. Lin, *Adv. Funct. Mater.* **17**, 1225 (2007).

[10] M. Vallet-Regi, F. Balas, D. Across, *Angew. Chem. Int. Ed.* **46**, 7548 (2007).

[11] B.G. Trewyn, I.I. Slowing, S. Giri, H.T. Chen, V.S.Y. Lin, *Acc. Chem. Res.* **40**, 846 (2007).

[12] P. Yang, M. Lu, D. Xu, D. Yuan, G. Zhou, *Appl. Phys. A.* **73**, 455 (2001).

[13] W. Sang, Y. Qian, J. Min, D. Li, L. Wang, W. Shi, L. Yinfeng, *Solid State Commun.* **121**, 475 (2002).

[14] Bohua Dong, Lixin Cao, Ge Su, Wei Liu, Hua Qu, Daixun Jiang, *J. Colloid Int. Sci.* **339**, 78 (2009).

[15] N. Uzar, S. Okur, M.C. Arikan, *Sens. Actuat. A Phys.* **167**, 188 (2011).

[16] L. Luo, H. Chen, L. Zhang, K. Xu, Y. Lv, *Anal. Chim. Acta* **635**, 183 (2009).

[17] M. Geszke, M. Murias, L. Balan, G. Medjahdi, J. Korczynski, M. Moritz, J. Lulek, R. Schneider, *Acta Biomater.* **7**, 1327 (2011).

[18] Z.G. Zhao, F.X. Geng, T. Congh, J.B. Bai, H.M. Cheng, *Nanotechnology* **17**, 4731 (2006).

[19] Y.D. Li, Y. Ding, Y. Zhang, Y.T. Qian, *J. Phys. Chem. Solids* **60**, 13 (1999).

[20] S.-H. Yu, M. Yoshimura, *Adv. Mater.* **14**, 296 (2002).

[21] J.P. Li, Y. Xu, D. Wu, Y.H. Sun, *Solid State Commun.* **130**, 619 (2004).

[22] M. Azad Malik, N. Revaprasadu, P. O'Brien, *Chem. Mater.* **13**, 913 (2001).

[23] W. Liu, *Mater. Lett.* **60**, 551 (2006).

[24] A.K. Verma, T.B. Rauchfuss, S.R. Wilson, *Inorg. Chem.* **34**, 3072 (1995).

[25] A.H. Souici, N. Keghouche, J.A. Delaire, H. Remita, M. Mostafavi, *Chem. Phys. Lett.* **422**, 25 (2006).

[26] P.K. Ghosh, S. Jana, S. Nandy, K.K. Chattopadhyay, *Mater. Res. Bull.* **42**, 505 (2007).

[27] J. Nanda, S. Sapra, D.D. Sarma, N. Chandrasekharan, G. Hodes, *Chem. Mater.* **12**, 1018 (2000).

[28] W. Vogel, P.H. Borse, N. Deshmukh, S.K. Kulkarni, *Langmuir* **16**, 2032 (2000).

[29] X. Zhang, H. Song, L. Yu, T. Wang, X. Ren, X. Kong, Y. Xie, X. Wang, *J. Lumin.* **118**, 251 (2006).

[30] J. Zhang, Z. Lin, Y. Lan, G. Ren, D. Chen, F. Huang, M. Hong, *J. Am. Chem. Soc.* **128**, 12981 (2006).

[31] J. Joo, H.B. Na, T. Yu, J.H. Yu, Y.W. Kim, F. Wu, J.Z. Zhang, T. Hyeon, *J. Am. Chem. Soc.* **125**, 11100 (2003).

[32] J. Hasanzadeh, S. Farjami Shayesteh, *Opt. Appl.* **XLI**, 921 (2011).

[33] L.E. Brus, *J. Chem. Phys.* **80**, 4403 (1984).

[34] Y.S. Yuang, F.Y. Chen, Y.Y. Lee, C.L. Liu, *J. Appl. Phys.* **76**, 3041 (1994).

[35] Landolt-Bornstein, *Numerical Data and Functional Relationships in Science and Technology*, Vol. 22a, Springer Verlag, Berlin 1987, p. 168.

[36] J. Hasanzadeh, A. Taherkhani, M. Ghorbani, *Chin. J. Phys.* **51**, 540 (2013).

[37] A.D. Dinsmore, D.S. Hsu, S.B. Qadri, J.O. Cross, T.A. Kennedy, H.F. Gray, B.R. Ratna, *J. Appl. Phys.* **88**, 4985 (2000).

[38] J.M. Hwang, M.O. Oh, I. Kim, J.K. Lee, C.S. Ha, *Curr. Appl. Phys.* **5**, 31 (2005).